Available online at www.sciencedirect.com
ScienceDirect
Journal of Magnetic Resonance 190 (2008) 255–270
JMR Journal of Magnetic Resonance
www.elsevier.com/locate/jmr

Anomalous diffusion expressed through fractional order differential operators in the Bloch–Torrey equation

Richard L. Magin [a,*], Osama Abdullah [a], Dumitru Baleanu [b,c], Xiaohong Joe Zhou [a,d]

[a] Department of Bioengineering, University of Illinois at Chicago, 851 South Morgan Street, Chicago, IL 60607-7052, USA
[b] Department of Mathematics and Computer Sciences, Faculty of Arts and Sciences, Cankaya University, Ankara, Turkey
[c] Institute of Space Sciences, Bucharest, Romania
[d] Departments of Radiology and Neurosurgery and Center for Magnetic Resonance Research, University of Illinois at Chicago, Chicago, IL, USA

Received 15 June 2007; revised 8 November 2007
Available online 13 November 2007

Abstract

Diffusion weighted MRI is used clinically to detect and characterize neurodegenerative, malignant and ischemic diseases. The correlation between developing pathology and localized diffusion relies on diffusion-weighted pulse sequences to probe biophysical models of molecular diffusion—typically $\exp[-(bD)]$—where D is the apparent diffusion coefficient (mm^2/s) and b depends on the specific gradient pulse sequence parameters. Several recent studies have investigated the so-called anomalous diffusion stretched exponential model—$\exp[-(bD)^{\alpha}]$, where α is a measure of tissue complexity that can be derived from fractal models of tissue structure. In this paper we propose an alternative derivation for the stretched exponential model using fractional order space and time derivatives. First, we consider the case where the spatial Laplacian in the Bloch–Torrey equation is generalized to incorporate a fractional order Brownian model of diffusivity. Second, we consider the case where the time derivative in the Bloch–Torrey equation is replaced by a Riemann–Liouville fractional order time derivative expressed in the Caputo form. Both cases revert to the classical results for integer order operations. Fractional order dynamics derived for the first case were observed to fit the signal attenuation in diffusion-weighted images obtained from Sephadex gels, human articular cartilage and human brain. Future developments of this approach may be useful for classifying anomalous diffusion in tissues with developing pathology.

Keywords: Anomalous diffusion; Bloch–Torrey equation; Fractional calculus; Diffusion-weighted MRI; Stretched exponential

1. Introduction

The Bloch equation is a phenomenological description of the precessional motion and relaxation of the magnetization arising from nuclear magnetic moments—spins. Solving the Bloch equation for different combinations of static, radiofrequency and gradient magnetic fields provides the basis for NMR spectroscopy and MRI [1,2]. In each case the spin dynamics are orchestrated to emphasize a characteristic feature of the molecule, tissue or organism under study. In MRI, for example, the Bloch equation is solved sequentially to shape the excitation RF pulse for slice selection, to design feature specific pulse sequences for optimal sensitivity and contrast, and to encode flow, diffusion or perfusion via gradient manipulation [3,4]. The validity of the derived techniques is now well established in MRI for static magnetic fields up to 10 T [5], and for systems acquiring images in times as short as 10 milliseconds [6].

As MRI is applied with increasing temporal and spatial resolution, the spin dynamics are being examined more closely; such examinations extend our knowledge of biological materials through a detailed analysis of relaxation time distribution and water diffusion heterogeneity. Here the dynamic models become more complex as they attempt to correlate new data with a multiplicity of tissue compartments where processes are often anisotropic. Conventional wisdom extends the analysis using the Bloch equation from

* Corresponding author. Fax: +1 312 996 5921.
E-mail address: rmagin@uic.edu (R.L. Magin).

1090-7807/$ - see front matter © 2007 Elsevier Inc. All rights reserved.
doi:10.1016/j.jmr.2007.11.007

single exponential to multi-exponential behavior, and from single parameter diffusion to multi-compartmental diffusion and diffusion tensor imaging. Recently, Bennett and co-workers [7,8] presented a new method for describing diffusion in MRI using the so called "stretched exponential" function (e.g., $\exp[-(bt)^{\alpha}]$, where α is an arbitrary real number between zero and one) to fit the experimental data. Such functions have interesting properties, and have frequently been used in physics to describe non-exponential behavior [9,10]. Nevertheless, in NMR the novel feature of this approach is not that it provides an alternative function for curve fitting, but that it suggests a new way to connect nanoscale models of porous materials and tissues—in most studies using fractals—with observable NMR relaxation and diffusion processes [11–17].

Fractional order dynamics in physics—particularly when applied to diffusion—leads to an extension of the concept of Brownian motion through a generalization of the Gaussian probability function to what is termed anomalous diffusion (sub and super diffusion), where the statistical description of mean displacement (in one dimension) follows the relationship $\langle \Delta x^2 \rangle = 2Dt^{2H}$, where D is the diffusion coefficient and $H = 1/2$ for normal diffusion ($H > 1/2$ for super-diffusion, and $H < 1/2$ for sub-diffusion) [18–20]. The parameter H can be connected on one hand to the fractal dimension of the lattice or matrix over which diffusion occurs, and on the other hand to the order of the differential operator in a generalized fractional order diffusion equation. For example, if $C(x,t)$ represents the concentration of the diffusing species in one dimension, then a fractional order partial differential equation of the form

$$\frac{\partial^{\alpha} C(x,t)}{\partial t^{\alpha}} = D' \frac{\partial^{2\beta} C(x,t)}{\partial |x|^{2\beta}} \tag{1}$$

emerges (for real numbers α and β) from Fick's first law and the continuity equation [18,19], where D' is the generalized diffusion coefficient with units of $\mathrm{mm}^{2\beta}/\mathrm{s}^{\alpha}$. This time and space fractional generalization of the diffusion equation—like its integer order analog—has an equivalent formulation as the governing equation for the probability density function for so-called anomalous diffusion [21,22]. Anomalous diffusion arises when the continuous time random walk model is generalized both in time and in space. In time, the generalization takes the fractional form through the introduction of a jump waiting time that exhibits an inverse power law distribution, while in space the fractional order generalization follows from the introduction of a similar inverse power law distribution of jump lengths. In particular, the so called Levy flight is equivalent to the Riesz fractional order space operator. Thus the fractional order operators of fractional calculus have a direct representation in the extended stochastic models of the conventional random walk.

Analysis of diffusion problems in chemistry, physics and biophysics using such fractional order models, ($\alpha \sim 1$, $\beta \sim 1$), while not widely known, is extensive with recent books [9,10,23], conferences [24–26], and special issues of journals [27–31] addressing the approach. In NMR, for example, Köpf and co-workers have developed fractional order models for the anomalous diffusion of water in both normal and cancerous tissues [32]. In these studies the stretched exponential function (as well as a Rigaut-type asymptotic fractal) was shown to describe the NMR echo amplitude acquired using a stimulated echo within the fringe field of a 9.4 T NMR spectrometer. More recently, Bennett and co-workers [8] demonstrated that the stretched exponential function not only fits the diffusion data from human brain tissue more precisely, but that the parameter α, which they call the "heterogeneity index," reflected the microscopic tissue structure. A connection between α and tissue structure was also suggested in the recent publication of Özarslan and co-workers [33]. In that study, q-space spectroscopic NMR experiments were analyzed using fractal diffusion theory, probabilistic models of diffusion, and the projection/propagator formalism to model the NMR echo intensity in normal human brain gray matter, glioblastoma tissues, and human erythrocyte ghosts. In this paper, Özarslan linked the mean-square displacement of water with the fractal dimension (H), where $H = 1/d_{\mathrm{w}}$ and d_{w} is the fractal dimension of the Brownian motion path of the random walk assumed to underlie the observed diffusional behavior ($d_{\mathrm{w}} > 2$ indicates sub-diffusion; results in [33] showing d_{w} for gray matter > glioblastoma > erythrocyte ghosts). In the context of the success of such fractal order models for describing diffusion in complex biological tissues, and in the expectation that such models could provide a specific measure of changes in tissue due to development or disease, we were curious to examine the connection between fractional order dynamics and diffusion.

In this paper we show that the stretched exponential model follows from a fundamental extension of the Bloch–Torrey equation through application of the operators of fractional calculus. Specifically, we show that fractional order generalization of the integer order time and space derivatives in the Bloch–Torrey equation establishes a formalism involving mathematically well posed fractional order differential equations that yield solutions, which naturally exhibit power law behavior in the arguments of their solutions. These results suggest a justification for using fractal and multi-scale analysis in NMR and MRI and have the potential to be more widely applied as the instruments continue to evolve and as the analytical methods of fractional calculus mature.

2. Theory

The extension of the Bloch equation through the generalization of the time derivative of the magnetization to fractional order suggests a number of interesting possibilities concerning spin dynamics and magnetization relaxation. Since in this paper we are considering changes in signal intensity only due to diffusion, we will set aside

discussion of fractional order precession and generalized, that is, non-exponential, T_1 and T_2 relaxation, and focus on the Bloch–Torrey equation in the rotating frame. This approach follows that given by Abragam [1] and Haacke et al. [2] where the spin dynamics of the magnetization $\mathbf{M}(\boldsymbol{r},t)$ in the B_0 rotating frame are described by the equation

$$\frac{\partial \mathbf{M}(\boldsymbol{r},t)}{\partial t} = \gamma \mathbf{M}(\boldsymbol{r},t) \times \mathbf{B} + D\nabla^2 \mathbf{M}(\boldsymbol{r},t). \tag{2}$$

In this analysis T_1 and T_2 relaxations are neglected and $\boldsymbol{B}$ is assumed to be only a function of time-varying magnetic field gradients $\boldsymbol{G}(t)$, hence $\boldsymbol{B} = (\boldsymbol{r}\cdot\boldsymbol{G})\hat{z}$, $\boldsymbol{r} = x\hat{\boldsymbol{x}} + y\hat{\boldsymbol{y}} + z\hat{\boldsymbol{z}}$, ∇^2 is the Laplacian operator, $\nabla^2 = \partial^2_{xx} + \partial^2_{yy} + \partial^2_{zz}$, and γ and D are the gyromagnetic ratio (42.58 MHz/T for protons) and the diffusion coefficient (typically, 2×10^{-3} mm^2/s for water at room temperature), respectively.

For $M_{xy}(\mathbf{r},t) = M_x(\mathbf{r},t) + \mathrm{i}M_y(\mathbf{r},t)$, where $\mathrm{i} = \sqrt{-1}$, the transverse components of the magnetization obey the equation

$$\frac{\partial M_{xy}(\boldsymbol{r},t)}{\partial t} = -\mathrm{i}\gamma(\boldsymbol{r}\cdot\mathbf{G})M_{xy}(\boldsymbol{r},t) + D\nabla^2 M_{xy}(\boldsymbol{r},t). \tag{3}$$

Assume a solution to this partial differential equation of the form

$$\boldsymbol{M}_{xy}(\boldsymbol{r},t) = M_0 A(t)\exp\left[-\mathrm{i}\gamma\boldsymbol{r}\cdot\int_0^t \mathbf{G}(t')\,\mathrm{d}t'\right], \tag{4}$$

where $M_{xy}(\boldsymbol{r},0) = M_0$ and $A(0) = 1$. Substitution of Eq. (4) into Eq. (3) gives

$$\frac{1}{A(t)}\left\{\frac{\mathrm{d}A(t)}{\mathrm{d}t}\right\} = \mathrm{e}^{\mathrm{i}\gamma r\cdot\int_0^t \mathbf{G}(t')\,\mathrm{d}t'} D\nabla^2\left[\mathrm{e}^{-\mathrm{i}\gamma r\cdot\int_0^t \mathbf{G}(t')\,\mathrm{d}t'}\right], \tag{5}$$

which after applying the Laplacian operator and integrating can be expressed as

$$\ln A(t) = -D\gamma^2\int_0^t\left[\left(\int_0^{t'}\mathbf{G}(t'')\,\mathrm{d}t''\right)\cdot\left(\int_0^{t'}\mathbf{G}(t'')\,\mathrm{d}t''\right)\right]\mathrm{d}t'. \tag{6}$$

This equation yields $M_{xy}(\boldsymbol{r},t)$ for specific gradient waveforms in the pulse sequence. For example, for a z-component spatial gradient $\mathbf{G}(t) = G_z(t)\hat{\mathbf{z}}$, the results [1–4] for a constant field gradient (G_z), a bipolar gradient pulse of duration T_b ($+G_z$ for $0 < t < T_b/2$; $-G_z$ for $T_b/2 < t < T_b$), or a Stejskal–Tanner gradient pulse pair each of duration δ, amplitude G_z, and separation by interval Δ are, respectively:

$$M_{xy} = M_0\exp(-\mathrm{i}\gamma G_z z t - (D\gamma^2 G_z^2 t^3/3)), \tag{7a}$$

$$M_{xy} = M_0\exp(-2D\gamma^2 G_z^2 T_b^3/3), \tag{7b}$$

$$M_{xy} = M_0\exp(-D\gamma^2 G_z^2\delta^2(\Delta - \delta/3)). \tag{7c}$$

Normally the argument of the exponential function in Eq. (7c) is written as $(-bD)$ where $b = (\gamma G_z\delta)^2(\Delta - \delta/3)$ and has the units of s/mm^2. When $\Delta >> \delta$, b can be approximated as $(\gamma G_z\delta)^2\Delta$.

Assume that a fractional order generalization of the Bloch–Torrey equation for the transverse magnetization in the rotating frame can be written as

$$\tau^{\alpha-1}\,{}_0{}^C D_t^\alpha M_{xy}(\boldsymbol{r},t) = \lambda M_{xy}(\boldsymbol{r},t) + D\mu^{2(\beta-1)}\nabla^{2\beta}M_{xy}(\boldsymbol{r},t), \tag{8}$$

where $\lambda = -\mathrm{i}\gamma(\boldsymbol{r}\cdot\boldsymbol{G}(t))$, ${}_0{}^C D_t^\alpha$ is the Caputo form of the Riemann–Liouville fractional order derivative in time [34,35], $\nabla^{2\beta} = (D_x^{2\beta} + D_y^{2\beta} + D_z^{2\beta})$ is a sequential Riesz fractional order Laplacian operator in space [34,36], (also, see the Appendix for formal definitions of these linear differential operators), and $\tau^{\alpha-1}$ and $\mu^{2(\beta-1)}$ are fractional order time and space constants needed to preserve units, ($0 < \alpha \leqslant 1$, and $1/2 < \beta \leqslant 1$). When $\alpha = 1$ and $\beta = 1$ the fractional differential operators conform with the usual integer order time and space partial derivatives, and the classical Bloch–Torrey equation is recovered. Note that the operators $(D_x^{2\beta}, D_y^{2\beta}, D_z^{2\beta})$ represent the sequential Riesz fractional order derivatives with respect to space and should be distinguished from diffusion coefficients used elsewhere.

We will consider two simple cases: (1) $\alpha = 1$ and $1/2 < \beta < 1$, where the diffusion term is assumed to follow fractional order dynamics in space, and (2) $0 < \alpha < 1$ and $\beta = 1$, where the spin dynamics are assumed to follow fractional order behavior in time.

(Case I) Fractional order dynamics in space

In this case ($\alpha = 1, \beta$ an arbitrary real number, $1/2 < \beta < 1$) the transverse magnetization must satisfy the equation

$$\frac{\partial M_{xy}(\boldsymbol{r},t)}{\partial t} = \lambda M_{xy}(\boldsymbol{r},t) + D\mu^{2(\beta-1)}\nabla^{2\beta}M_{xy}(\boldsymbol{r},t). \tag{9}$$

Following the steps in the analysis given above for the $\beta = 1$ case, we obtain

$$\frac{\mathrm{d}}{\mathrm{d}t}[\ln A(t)] = \mathrm{e}^{\mathrm{i}2\pi\boldsymbol{r}\cdot\boldsymbol{k}(t)} D\mu^{2(\beta-1)}\nabla^{2\beta}[\mathrm{e}^{-\mathrm{i}2\pi\boldsymbol{r}\cdot\boldsymbol{k}(t)}], \tag{10}$$

where $\mathbf{k}(t) = (\gamma/2\pi)\int_0^t \mathbf{G}(t')\,\mathrm{d}t'$. First, considering only the $D_x^{2\beta}$ term of the fractional order Laplacian with $a = -2\pi k_x(t)$, we must evaluate the sequential Riesz fractional order space derivative

$$D_x^{2\beta}[\mathrm{e}^{\mathrm{i}ax}] = D_x^\beta\{D_x^\beta[\mathrm{e}^{\mathrm{i}ax}]\}. \tag{11}$$

Each derivative can be determined for well behaved functions, using

$$D_x^\beta[\mathrm{e}^{\mathrm{i}ax}] = F^{-1}\{|\xi_x|^\beta F\{\mathrm{e}^{\mathrm{i}ax}\}\} = |a|^\beta\mathrm{e}^{\mathrm{i}ax}, \tag{12}$$

where F represents the spatial Fourier transform (defined in the Appendix) in terms of the spatial frequency ξ_x.

Similarly, applying this definition for the y and z component of $\mathrm{e}^{-\mathrm{i}2\pi\boldsymbol{r}\cdot\boldsymbol{k}(t)}$ and substitution into Eq. (10) gives

$$\frac{\mathrm{d}}{\mathrm{d}t}[\ln A(t)] = -D\mu^{2(\beta-1)}(2\pi)^{2\beta}[(k_x(t))^{2\beta} + (k_y(t))^{2\beta} + (k_z(t))^{2\beta}], \tag{13}$$

which after integration becomes

$$\ln A(t) = -D\mu^{2(\beta-1)}(2\pi)^{2\beta}\int_0^t [(k_x(t'))^{2\beta} + (k_y(t'))^{2\beta} + (k_z(t'))^{2\beta}]\,\mathrm{d}t'. \tag{14}$$

Note that this equation corresponds to the classical result

$$\ln A(t) = -D(2\pi)^2\int_0^t [\boldsymbol{k}(t')\cdot\boldsymbol{k}(t')]\,\mathrm{d}t', \tag{15}$$

for $\beta = 1$.

If we again consider only a single spatial gradient $\mathbf{G}(t) = \mathbf{G}_z(t)\hat{\mathbf{z}}$, then for fixed, bipolar, and Stejskal–Tanner gradient pulses, as defined above, we find:

$$M_{xy} = M_0\exp(-\mathrm{i}\gamma G_z z t - D\mu^{2(\beta-1)}\gamma^{2\beta}G_z^{2\beta}t^{2\beta+1}/(2\beta+1)), \tag{16a}$$

$$M_{xy} = M_0\exp(-2D\mu^{2(\beta-1)}\gamma^{2\beta}G_z^{2\beta}T_b^{2\beta+1}/(2\beta+1)), \tag{16b}$$

$$M_{xy} = M_0\exp\left[-D\mu^{2(\beta-1)}(\gamma G_z\delta)^{2\beta}\left(\Delta - \frac{2\beta-1}{2\beta+1}\delta\right)\right]. \tag{16c}$$

Again, the classical results given in Eq. (7) are recovered in each case for $\beta = 1$.

(Case II) Fractional order dynamics in time

In this case (α an arbitrary real number, $0 < \alpha < 1$, $\beta = 1$) the transverse magnetization must satisfy

$$\tau^{\alpha-1}\,{}_0{}^{C}D_t^{\alpha}M_{xy}(\boldsymbol{r},t) = \lambda M_{xy}(\boldsymbol{r},t) + D\nabla^2 M_{xy}(\boldsymbol{r},t). \tag{17}$$

Following the standard analysis [1,2] we set $D = 0$ and solve

$$\tau^{\alpha-1}\,{}_0{}^{C}D_t^{\alpha}M_{xy}(\boldsymbol{r},t) + i\gamma(\boldsymbol{r}\cdot\boldsymbol{G}(t))M_{xy}(\boldsymbol{r},t) = 0 \tag{18}$$

with $M_{xy}(\mathbf{r},0) = M_0$ as the initial condition. However, although a unique solution to this equation can be proven to exist, this fractional order differential equation does not have a closed form analytical solution for an arbitrary gradient $\boldsymbol{G}(t)$ (see the monograph by Kilbas et al. [34] for a discussion of the existence and uniqueness conditions for the solution to fractional order differential equations using a generalized method of Frobenius).

In this paper we will consider only the simplest case of a constant, z-gradient $\mathbf{G}(t) = G_z\hat{\mathbf{z}}$ to illustrate the emergence of fractional order exponential decay in the signal amplitude. Using Eq. (18) with $D = 0$, we find

$$M_{xy}(\boldsymbol{r},t) = AE_\alpha[-\mathrm{i}\gamma z G_z\tau(t/\tau)^\alpha] = M_o E_\alpha[\lambda_z' t^\alpha], \tag{19}$$

where $M_{xy}(\boldsymbol{r},0) = A = M_0$ and $\lambda_z' = -\mathrm{i}\gamma z G_z\tau^{1-\alpha}$. Note here, that $\gamma z G_z\tau$ has the units of radians and that $E_\alpha(\lambda_z' t^\alpha)$ is the single parameter Mittag-Leffler function (the basic properties of this function are listed in the Appendix, but notice that $E_\alpha(\lambda_z' t^\alpha) = \exp(\lambda_z' t)$ when $\alpha = 1$).

Generalization of A to $A(t)$ and substitution of Eq. (19) into Eq. (17) gives

$${}_0{}^{C}D_t^{\alpha}[A(t)E_\alpha(\lambda_z' t^\alpha)] = \lambda_z'[A(t)E_\alpha(\lambda_z' t^\alpha)] + D\tau^{1-\alpha}\nabla^2[A(t)E_\alpha(\lambda_z' t^\alpha)]. \tag{20}$$

The Leibniz rule for fractional order derivatives [33] can be written as

$${}_0{}^{C}D_t^{\alpha}[\phi(t)f(t)] = \sum_{k=0}^{\infty}\binom{\alpha}{k}\phi^{(k)}(t)\,{}_0{}^{C}D_t^{\alpha-k}f(t), \quad \text{where } \binom{\alpha}{k} = \frac{\Gamma(\alpha+1)}{k!\Gamma(\alpha-k+1)}, \tag{21}$$

and $\phi(t)$ and $f(t)$, together with all their time derivatives, are continuous on $[0, t]$. In this expression, $\Gamma(z)$ is the gamma function as defined in the Appendix. This series can be used to expand the left side of Eq. (19). When the series is truncated for $k > 1$ and under the condition $t < \tau$ (see Appendix) we obtain

$$A(t)\,{}_0{}^{C}D_t^{\alpha}[E_\alpha(\lambda_z' t^\alpha)] + \alpha\frac{\mathrm{d}A(t)}{\mathrm{d}t}\,{}_0{}^{C}D_t^{\alpha-1}[E_\alpha(\lambda_z' t^\alpha)] = \lambda_z' A(t)E_\alpha[\lambda_z' t^\alpha] + D\tau^{1-\alpha}A(t)\frac{\mathrm{d}^2}{\mathrm{d}z^2}[E_\alpha(\lambda_z' t^\alpha)]. \tag{22}$$

Evaluation of the fractional and integer order derivatives (and the fractional order integral) of the single parameter Mittag-Leffler function in Eq. (19) is given in the Appendix. Using those results, we find

$$\frac{1}{A(t)}\frac{\mathrm{d}A(t)}{\mathrm{d}t} = \frac{2D\tau^{1-\alpha}a^2t^{2\alpha}E_{\alpha,2\alpha+1}^3(azt^\alpha)}{\alpha t^{1-\alpha}E_{\alpha,2-\alpha}(azt^\alpha)}, \tag{23}$$

where $a = -\mathrm{i}\gamma G_z\tau^{1-\alpha}$. Assuming $(t/\tau) << 1$, we can approximate the two parameter Mittag-Leffler functions by the first terms of their power series representation to yield

$$\frac{\mathrm{d}}{\mathrm{d}t}[\ln A(t)] = \frac{-2D\gamma^2G_z^2(\tau^{1-\alpha})^3t^{3\alpha-1}\Gamma(2-\alpha)}{\alpha\Gamma(2\alpha+1)}, \tag{24}$$

which following integration with $A(0) = 1$ can be written as

$$A(t) = \exp[-B(t/\tau)^{3\alpha}], \quad \text{where } B = \frac{2\Gamma(2-\alpha)D\gamma^2G_z^2\tau^3}{3\alpha^2\Gamma(2\alpha+1)}. \tag{25}$$

Finally, for the case of a fixed G_z gradient we obtain

$$M_{xy} = M_0E_\alpha[-\mathrm{i}\gamma G_z z\tau(t/\tau)^\alpha]\exp[-B(t/\tau)^{3\alpha}]. \tag{26}$$

For $\alpha = 1$ this result reduces to the classical case of attenuation in a constant field gradient that is given in Eq. (7a).

3. Methods

Three diffusion-weighted MRI experiments were carried out to illustrate applications of the Case I theoretical analysis. The first two experiments were conducted at 11.74 T (500 MHz for protons) using a 56 mm vertical bore magnet (Oxford Instruments, Oxford, UK) and a Bruker DRX Avance Spectrometer (Bruker Instruments, Billerica, MA. USA). MR images were acquired using a Bruker Micro 5 imaging probe with triple axis gradients (maximum

strength 2000 mT/m). A 5 mm diameter Bruker RF saddle coil was used to transmit RF energy to excite the spins and to receive the nuclear magnetic resonance signals. The third experiment was carried out using a clinical MRI scanner operating at 3.0 T (Signa HDx; General Electric Health Care, Milwaukee, Wisconsin), with a quadrature birdcage RF coil and a gradient coil system capable of producing a linear gradient up to a value of 40 mT/m.

3.1. 11.74 T Diffusion-weighted imaging experiments

The first experiment was conducted using glass capillary tubes filled with Sephadex (Sigma-Aldrich, St. Louis, MO) gels. Sephadex is a dextran polymer that swells in water to form a gel with many small interconnecting pores. In this study, three types of superfine Sephadex particles (dry particle diameter 20–50 μm) were used: G-25, G-50 and G-100. The powder was hydrated for more than 72 h at room temperature in three separate beakers using distilled water as a solvent. The gels were carefully drawn into three capillary tubes (inner diameter of 1.2 mm) so that no air bubbles were trapped. After the gels were allowed to settle, the capillary tubes were sealed at both ends, and placed in a 5 mm NMR tube filled with distilled water. Diffusion-weighted images were acquired using a Stejskal–Tanner diffusion-weighted spin–echo pulse sequence with the following parameters: TR = 1000 ms, TE = 60 ms, slice thickness = 1.5 mm, $\Delta = 45$ ms, $\delta = 1$ ms, and 4 averages. The FOV was 0.6 cm × 0.6 cm, which for a matrix size of 64×64 corresponds to an in-plane resolution of 94 μm × 94 μm. The diffusion weighting gradient was applied along the phase-encoding direction in eight steps to a maximum strength of 700 mT/m, which corresponds to a maximum b-value of 1600 s/mm^2. Diffusion gradients along the phase direction were used to minimize the interaction between the gradient pulses, which can generate cross-terms that affect signal attenuation [3,4].

The second experiment was conducted using human articular cartilage plugs. Human tali were obtained within 24 h of death of the donor through the Gift of Hope Organ and Tissue Donor Network (from Rush University with institutional review board approval), and frozen at −80 °C until experimentation. Full thickness cartilage tissue samples were harvested immediately prior to experimentation. The samples were first cut using a band saw with a diamond tip blade to eliminate any saw blade artifacts, and then trimmed to 3 mm cubes with a sharp scalpel blade. The cartilage/bone samples were placed in NMR sample tubes filled with physiologic saline. The NMR tubes were loaded into the 5-mm diameter RF saddle coil and inserted into the Bruker Micro5 imaging probe. Diffusion-weighted images were acquired using a Stejskal–Tanner diffusion-weighted spin–echo pulse sequence with the following parameters: TR = 1000 ms, TE = 30 ms, slice thickness = 1 mm, $\Delta = 25$ ms, $\delta = 1$ ms, and 4 averages. The FOV was 0.6 cm × 0.6 cm, which for a matrix size of 128×128 corresponds to an in-plane resolution of 47 μm × 47 μm. The diffusion weighting gradient was applied along the phase direction in fifteen steps with a maximum strength of 1100 mT/m, which corresponds to a maximum b-value of 2200 s/mm^2.

3.2. 3.0 T Diffusion-weighted imaging experiment

In the third experiment, diffusion-weighted brain imaging was carried out on a healthy human volunteer at the University of Illinois Medical Center using an institutional review board approved protocol. Axial images were acquired with multiple b-values using a customized single-shot EPI pulse sequence to minimize eddy current induced distortion [37]. The key data acquisition parameters were: TR = 4000 ms, TE = 96.6 ms, slice thickness of 4 mm, slice gap of 3 mm, $\Delta = 42.6$ ms, $\delta = 32.2$ ms, and 4 averages. The FOV was 22 cm × 22 cm, which for a matrix size of 128×72 (zero padded to 256×256 during image reconstruction) yielded a spatial resolution of 1.72 mm × 3.05 mm. Fourteen diffusion-weighted images were acquired with a maximum b-value of 3300 s/mm^2, as defined in Eq. (7c). At each b-value, the diffusion-weighting gradient was applied along the x, y, and z- axis, respectively, to obtain a trace-weighted image where the effect of diffusion anisotropy is minimized.

3.3. Image analysis for regions of interest (ROI)

In the first experiment, three individual ROIs (7–9 pixels each) were selected in the image for the G-25, G-50, G-100 Sephadex samples and for the distilled water region. In the second experiment, three individual ROIs (5–9 pixels depending on the specific zone) were selected in the superficial, middle, and deep zones, and from the surrounding saline medium. For the human brain experiment, two ROIs (left and right hemispheres) were selected from the CSF (3 pixels) and the white and gray matter (9 pixels) regions of the image. All ROI data were fit to the fractional order attenuation model, Eq. (16c) by using the Levenberg–Marquardt algorithm [38] implemented in MATLAB R14 (MathWorks Inc, Natick, MA) to estimate the parameters D, β and μ. This algorithm minimizes the cost function:

$$C = \sum_{i=1}^{n} (y_i - f(\vec{x}_i, \vec{a}))^2, \tag{27}$$

where y_i is the experimental diffusion data (normalized intensities) of length n, $f(\vec{x}_i, \vec{a})$ is defined in Eq. (16c) as a function of $\vec{x}_i = [G_z, \Delta, \delta]$ (independent variables) to evaluate the adjustable coefficients $\vec{a} = [D_f, \beta, \mu]$ in the least-squares sense. In applying the Levenberg–Marquardt algorithm, the upper bound for D_f was not allowed to exceed D_m obtained from the mono-exponential fit, i.e., $0 < D_f \leqslant D_m$, since the two values for the diffusion coefficient should converge for low b-values. The bounds on β and μ were taken as: $1/2 < \beta < 1$ and $0 < \mu < 500$ μm. The

averages of the ROIs and standard deviations were calculated for all fits.

4. Results

The generalization of the Bloch–Torrey equation using fractional calculus provides a mechanism for introducing fractional order dynamics in space (Case I) or time (Case II). In this section we present theoretical results for Case I and Case II and experimental findings for Case I applied to diffusion-weighted images of Sephadex gels, human cartilage and the human brain. In the theoretical study, the derived magnetization attenuation curves are compared with the classical result and a more recent expression derived using fractal models. In the experimental study, the decay of image intensity for increasing b-values was fit to selected ROI. The gel and tissue samples were chosen to illustrate key features of the theory and to demonstrate the theory's applicability to diffusion in simple and complex materials.

The theoretical curves were plotted versus the gradient parameter b (where for $\Delta >> \delta$, $b = (\gamma\ G_z\delta)^2\Delta$) for Case I ($\alpha = 1$) for selected values of β and μ, and as a function of time (TE or t) for fixed β and selected μ. For Case II ($\beta = 1$) the magnetization decay curves are plotted versus time for fixed G_z and α and for selected values of τ. As an example of the behavior expected in Case I, the decay of the normalized magnetization ($M_{xy}(b)/M_0$), as given in Eq. (16c), is plotted in Fig. 1 for a fixed value of the diffusion coefficient (D) for different values of β (0.6–1.0 in steps of 0.1). In this figure a Stejskal–Tanner gradient pulse sequence (G_z, Δ, δ) is assumed with G_z varying from 0 to 1500 mT/m. In this example, we observe that as β decreases from 1.0 to 0.6 the attenuation curves change from a simple exponential—a straight line on the semi-log graph—to a curved shape that strongly resembles the behavior recorded in restricted diffusion—particularly at high b-values. In Fig. 2, Eq. (16c) is plotted for a series of μ values ranging from 20 to 80 μm with $\beta = 0.8$. The Δ, δ and G_z values in Fig. 2 are the same as those used in Fig. 1. Here we see that increasing the value of μ appears to increase the contribution of restricted diffusion in the diffusion attenuation curve for a fixed value of β. This behavior is evident when Eq. (16c) is expressed either in terms of a single exponential decay, $\exp[-bD_{\mathrm{apI}}]$, where the apparent diffusion coefficient in Case I is expressed as: $D_{\mathrm{apI}} = D/((\gamma G_z\delta)\mu)^{2(1-\beta)}$; or when Eq. (16c) is written as a stretched exponential, $\exp[-(bD_{\mathrm{F}})^{\beta}]$, where $D_{\mathrm{F}}^{\beta} = D(\Delta/\mu^2)^{1-\beta}$. In addition, when $\mu = \sqrt{D\Delta}$ the Case I theory corresponds exactly with the "stretched exponential" result, $\exp(-(bD)^{\beta})$, considered by Bennett [7,8]. In the example plotted in Fig. 2 this correspondence occurs for $\mu = 7.07$ μm. Overall, Figs. 1 and 2 show for Case I a decrease in the apparent diffusion coefficient as the values of β decrease and μ increase.

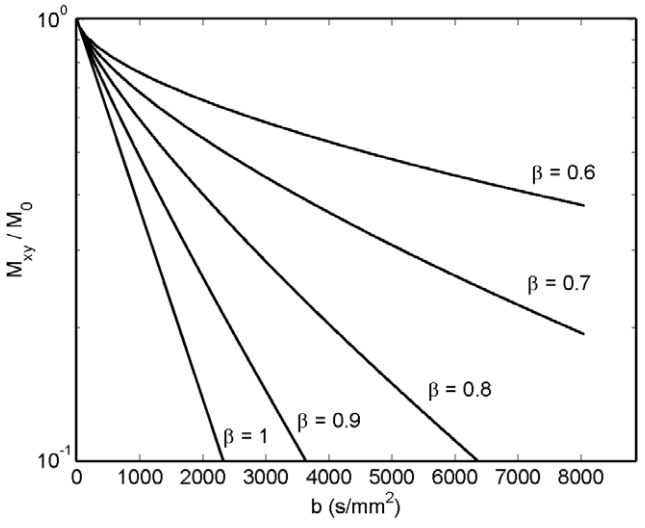

Fig. 1. Normalized decay of the transverse magnetization (according to Eq. (16c)), plotted versus b, where $b = (\gamma G_z\delta)^2\Delta$, for selected values of β. In each curve, G_z increases from 0 to 1500 mT/m while all other parameters are fixed: D (1×10^{-3} mm^2/s), Δ (50 ms), δ (1 ms) and μ (35 μm).

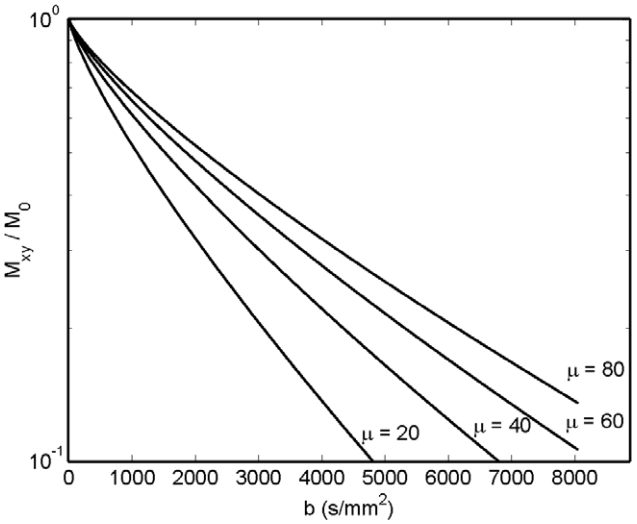

Fig. 2. Normalized decay of the transverse magnetization (according to Eq. (16c)), plotted versus b, where $b = (\gamma G_z\delta)^2\Delta$, with selected values of μ. In each curve, G_z increases from 0 to 1500 mT/m while all other parameters are fixed: D (1×10^{-3} mm^2/s), Δ (50 ms), δ (1 ms) and β (0.8).

The attenuation of the normalized transverse magnetization in the presence of a bipolar gradient, Case I, Eq. (16b), is plotted in Fig. 3 for a spin echo pulse sequence. In this figure, the expected echo attenuation as a function of the echo time (TE) is shown for $\beta = 0.6$, and μ values from 10 to 40 μm in steps of 10 μm. Also plotted in Fig. 3 is the classical single spin echo expression, $\exp[-D\gamma^2G_z^2\mathrm{TE}^3/12]$, originally derived by Hahn [1,2], and a theoretical expression for anomalous diffusion derived by Kärger, Pfeifer and Vojta [14]. In this situation just as seen in Fig. 1, increasing β values toward 1.0 collapses the theoretical curves given by Eq. (16b) into the classical result. For a fixed β value and the selected values of μ, the classical result appears to fall between the Kärger equation and the fractional order theory developed here. However, the time rate of decay (i.e., the power to which TE is raised) is different

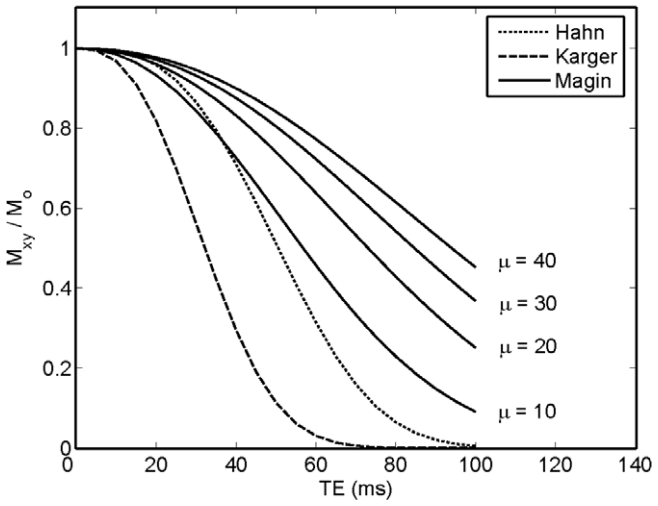

Fig. 3. Normalized decay of the transverse magnetization for a spin echo sequence (according to Eq. (16b)) plotted versus TE for selected values of μ with fixed G_z (30 mT/m), D (1×10^{-3} mm^2/s) and β(0.6). Also plotted are the classical result for a single echo, $\exp(-D\gamma^2G_z^2\mathrm{TE}^3/12)$, and an equation derived by Kärger et al. [14], $\exp(-D(1-2^{-\beta})\gamma^2G_z^2\mathrm{TE}^{\beta+2}/(\beta+1)(\beta+2))$, using an anomalous diffusion model in a fractal system, $\langle z^2(t)\rangle = 2Dt^{\alpha}$.

in each case; when $\beta = 0.5$ the Kärger equation predicts decay curves of the form $\exp[-a\mathrm{TE}^{2.5}]$, while the fractional order model gives $\exp[-b\mathrm{TE}^2]$, and the classical theory yields $\exp[-c\mathrm{TE}^3]$.

Fractional order generalization of the time derivative in the Bloch–Torrey equation (Case II) also predicts stretched exponential behavior. This is illustrated in Fig. 4, which is a plot of Eq. (25): the normalized time decay of transverse magnetization following application of a 90° pulse to spins in a fixed G_z gradient. The classical decay, $\exp[-D\gamma^2G_z^2t^3/3]$,

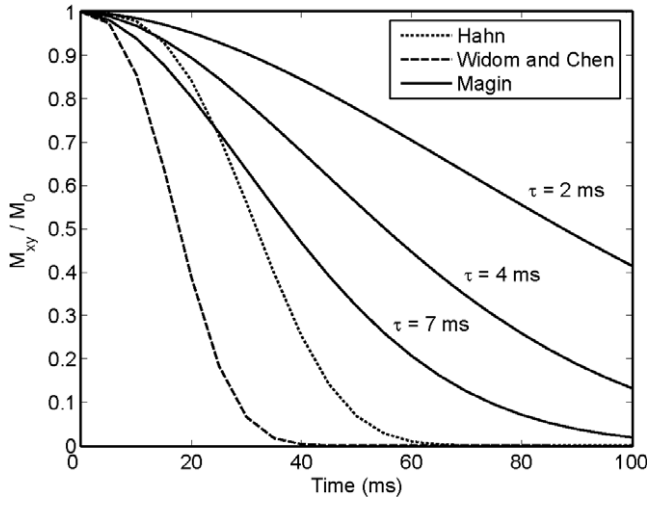

Fig. 4. Normalized decay of the transverse magnetization following application of a 90° pulse to spins in a constant z-gradient (according to Eq. (25)) plotted versus time for selected values of τ with fixed G_z (30 mT/m), $D(1\times10^{-3}$ mm^2/s) and α (0.6). Also plotted are the classical result derived by Hahn, $\exp(-D^{\alpha}\gamma^2G_z^2t^3/3)$, and the equation derived by Widom and Chen [15], $\exp(-D^{\alpha}\gamma^2G_z^2t^{2+\alpha}/(2+\alpha))$, for anomalous diffusion in a fixed gradient.

is compared with the fractional order theory when $\alpha = 0.6$ and τ values are set to 2, 4 and 7 ms. As the α values approach 1, the decay curves predicted by Eq. (25) again conform to the classical result (data not shown). Also plotted in Fig. 4 is an equation derived by Widom and Chen [15] for diffusion in a fractal medium. In the Widom and Chen model the exponential decay curve is given by $\exp[-D_{\mathrm{apWC}}\gamma^2G_z^2t^{2+\alpha}]$, with an apparent diffusion coefficient defined as $D_{\mathrm{apWC}} = D^{\alpha}/(2+\alpha)$, which depends on α—a measure of the fractal dimension of the material. On the other hand, for the fractional order model, the apparent diffusion coefficient depends on both α and τ^{α}, the fractional order time constant; that is, the exponential decay curve is given by $\exp[-D_{\mathrm{apII}}\gamma^2G_z^2t^{3\alpha}]$, with an apparent diffusion coefficient expressed as $D_{\mathrm{apII}} = 2(2-\alpha)\tau^{3(1-\alpha)}D/3\alpha^2\ \Gamma(2\alpha+1)$ for Case II. Note however, that in the Widom and Chen model D^{α} must have the units mm^2/(s)$^{1+\alpha}$, hence $D_{\mathrm{apWC}} = D\tau_{\mathrm{WC}}^{-\alpha}$ and a unit preserving time constant is also needed. The time decay curves for the fractional order model (Case II) and the Widom and Chen model for $\alpha = 1/2$ follow different exponential power law decays: $\exp[-a't^{2.5}]$ for the Widom and Chen model and $\exp[-b't^{1.5}]$ for the fractional order model. Both results are quite different from the $\exp[-c't^3]$ expected for spins undergoing unrestricted diffusion in a constant G_z gradient.

The signal attenuation in Sephadex gels (G-25, G-50 and G-100) at 11.74 T for a Stejskal–Tanner pulse gradient spin echo was measured for selected regions of interest (ROI) at increasing b values, and the data fit to the fractional order model (Eq. (16c)). Sephadex forms a dextran–water gel when the dry powder (20–50 μm, dia.) swells in water to form beads with many small interconnecting pores. The numerical value of the Sephadex refers to the approximate molecular exclusion size (in kiloDaltons, kDa) of the pores. Hence, molecules with a molecular weight greater than 25 kDa would be excluded from the interior of the G-25 gels. Since water can gain easy access to all pores, the Sephadex gel beads G-25, G-50, G-100 provide a graded series of water compartments with increasing effective pore size; a series exhibiting an increasing likelihood of unrestricted diffusion ($\beta \approx 1$). This behavior is in fact observed in the experimental curves shown in Fig. 5; the G-25 gel shows a normalized decay curve that is non-linear (on the logarithmic scale), while the G-100 is nearly as linear as the curve for the solvent (distilled water). The fractional order model was fit to the Sephadex data for selected ROI in the limit of $\Delta << \delta$ using Eq. (16c) with the signal assumed to be directly proportional to the transverse magnetization, hence, $S = S_0\exp[-(bD_{\mathrm{F}})^{\beta}]$ where $D_{\mathrm{F}}^{\beta} = D_{\mathrm{f}}(\Delta/\mu^2)^{1-\beta}$. In this experiment the D_{f}, β, and μ values were obtained using the Levenberg–Marquardt nonlinear least squares algorithm, as described in Section 3. For distilled water, $\beta = 1.0$, $\mu = 2.9$ μm and $D_{\mathrm{f}} = 2.1\times10^{-3}$ mm^2/s, whereas for G-25 we found $\beta = 0.71$, $\mu = 6.4$ μm and $D_{\mathrm{f}} = 1.2\times10^{-3}$ mm^2/s, with the corresponding values for G-50 and G-100 falling in between.

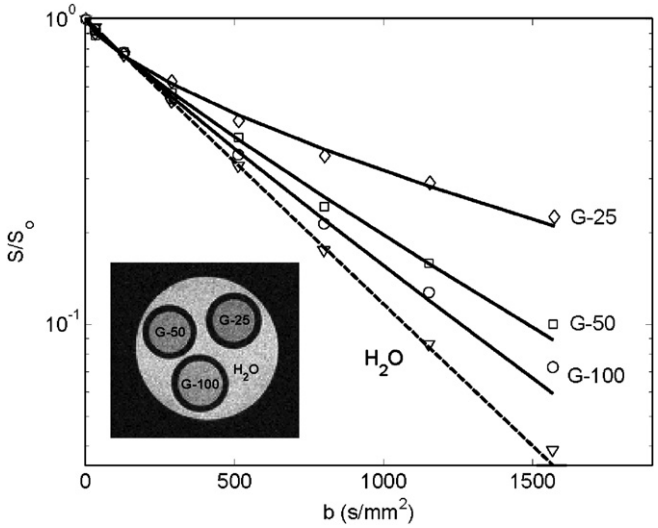

Fig. 5. Normalized signal intensity plotted versus b, where $b = (\gamma G_z \delta)^2 \Delta$, for selected ROI in samples of distilled water and Sephadex G-25, G-50 and G-100. The experimental data were fit to the fractional order model (Eq. (16c)) to determine D_f, β and μ for $\Delta = 45$ ms and $\delta = 1$ ms. The inset shows a T_2-weighted spin echo image of the sample at 11.74 T, TR/TE = 1000/60 ms, FOV = 0.6 cm × 0.6 cm, matrix = 64 × 64, in plane resolution = 94 μm × 94 μm, and slice thickness = 1.5 mm.

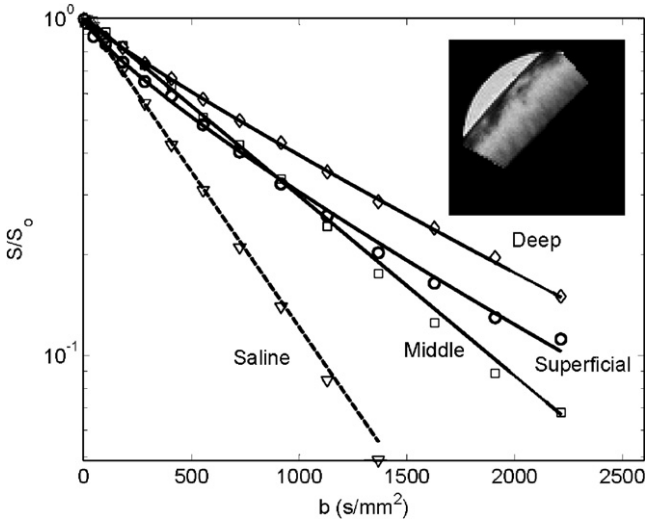

Fig. 6. Normalized signal intensity plotted versus b, where $b = (\gamma G_z \delta)^2 \Delta$, for selected ROI in the three different zones (superficial, middle and deep) of a human cartilage sample and in saline. The experimental data were fit to the fractional order stretched exponential model (Eq. (16c)) to determine D_f, β and μ for $\Delta = 25$ ms and $\delta = 1$ ms. The inset is a T_2-weighted spin echo image of the chondral plug at 11.74 T, TR/TE = 1000/30 ms, FOV = 0.6 cm × 0.6 cm, matrix = 128 × 128, in plane resolution = 47 μm × 47 μm and slice thickness = 1 mm.

These results confirm out hypothesis that the smaller the G-value of the Sephadex, the smaller the value of β and the larger the value of μ. A summary of the results for each of the Sephadex gels is listed in Table 1. Also shown in Table 1, for comparison, are results for the same data fit to a single exponential decay curve, $S = S_0 \exp[-bD_m]$. The observed changes in μ values do not directly reflect the increasing pore size in the series G-25, G-50, and G-100 because μ occurs in the denominator of the apparent fractional order diffusion coefficient D_F^β.

Articular cartilage consists of three distinct zones (superficial, middle and deep), each with a characteristic composition and structural organization of chrondocytes, collagen, proteoglycan and other smaller molecules [39]. The superficial zone has the highest water content with the collagen fibers generally oriented parallel to the articular surface. The middle zone is a transition region with high water content and a largely isotropic distribution of collagen. The collagen fibers in the deep zone are primarily orientated perpendicular to the calcified surface. The cartilage data shown in Fig. 6 was obtained for regions of interest (ROI) selected from a 1 mm slice in each zone. The signal attenuation curves for a Stejskal–Tanner pulse gradient were fit using the Levenberg–Marquardt nonlinear least squares algorithm as described in Section 3. A summary of the results is listed in Table 1. In the deep zone, for example, $D_f = 0.94 \times 10^{-3}$ mm^2/s, $\beta = 0.9$ and $\mu = 4$ μm. These results are consistent with the overall structure of cartilage; a structure that allows the water to freely diffuse in the middle zone, but restricts diffusion in the superficial and deep

Table 1
Summary of diffusion measurements

		$D_m \times 10^{-3}$ mm^2/s	$D_f \times 10^{-3}$ mm^2/s	β a.u.	μ (μm)
Sephadex	G25	1.2 ± 0.05	1.1 ± 0.04	0.71 ± 0.06	6.4 ± 0.1
	G50	1.7 ± 0.07	1.5 ± 0.03	0.8 ± 0.05	5.7 ± 0.1
	G100	2.0 ± 0.13	1.8 ± 0.06	0.91 ± 0.08	4.4 ± 1.6
	Distilled H$_2$O	2.2 ± 0.01	2.1 ± 0.02	1.0 ± 0.003	2.9 ± 0.3
Cartilage	Superficial	1.02 ± 0.09	1.01 ± 0.09	0.77 ± 0.006	4.3 ± 0.07
	Middle	1.24 ± 0.008	1.23 ± 0.008	1.0 ± 0.0	1.3 ± 0.02
	Deep	0.94 ± 0.03	0.94 ± 0.02	0.90 ± 0.01	4.3 ± 0.03
	Saline	2.13 ± 0.03	2.13 ± 0.03	1.0 ± 0.00	1.6 ± 0.07
Brain	White matter	0.41 ± 0.006	0.41 ± 0.006	0.60 ± 0.008	4.3 ± 0.04
	Gray Matter	0.76 ± 0.1	0.75 ± 0.08	0.78 ± 0.03	4.9 ± 0.02
	CSF	3.0 ± 0.0	2.8 ± 0.18	0.91 ± 0.005	3.0 ± 1.27

The D_m values were obtained from a least squares fit to the equation $S = S_0 \exp[-bD_m]$ while the D_f, β and μ values were found using the Levenberg–Marquardt nonlinear least square algorithm to fit Eq. (16c).

zones. The β values for the curve fits for the superficial, middle and deep zones were 0.77, 1.0 and 0.9, respectively. These values are consistent with the idea that the parameter β reflects the "complexity" of the tissue: lower β values correspond to more complex or heterogeneous tissues. The μ values for the three zones were: superficial, 4 μm; middle, 1 μm; and deep, 4 μm. The lower μ value in the middle zone is consistent with its model as a less restricted environment for water diffusion (decreasing μ in Eq. (16c) increases the apparent D_f). Note that the μ value of saline (1.3 μm) is slightly larger than the μ value found in the middle zone and smaller by almost a factor of two from the μ value found for distilled water in the Sephadex experiment. The variation of μ within experiments when β is near a value of one probably reflects uncertainty in the curve fit, while the between experiment difference is likely due to the different values of TE and Δ used in the two experiments. Additional studies are needed to investigate these findings.

Diffusion-weighted imaging (DWI) is increasingly used in clinical settings to characterize normal and compromised regions of the brain. In its simplest form, DWI uses the equation, $S = S_0\exp[-bD_{ap}]$, where D_{ap} is an apparent diffusion coefficient. Typically D_{ap} for both white and gray matter is significantly less than that of CSF (e.g., 0.76, 1.07 and 2.94×10^{-3} mm^2/s for gray, white matter with axial fiber orientation along **G**, and CSF, respectively) [3]. In addition, the white matter diffusion coefficient exhibits significant anisotropy: D_{ap} is larger along the direction of the fiber tracts than across them (1.07 versus 0.64×10^{-3} mm^2/s)—a fact used to map fiber tract directions. The diffusion attenuation data shown in Fig. 7 is taken from ROIs selected in white matter, gray matter and CSF of a human brain image acquired at 3 T (the inset shows an axial slice and the ROI). These data were fit to the fractional order model, Eq. (16c), using the Levenberg–Marquardt nonlinear least squares algorithm as described in Section 3, and the results are listed in Table 1. The β values follow the expected trend of decreasing in magnitude as the diffusion becomes more restricted; the β values for the gray matter and white matter were 0.78 and 0.6, respectively. The μ values were almost the same (approximately 5 μm). Both tissues exhibited restricted diffusion behavior in this experiment while an ROI taken in the CSF region gave an apparent single exponential decay ($D_f = 2.8\times10^{-3}$ mm^2/s, $\beta = 0.91$, $\mu = 3$ μm).

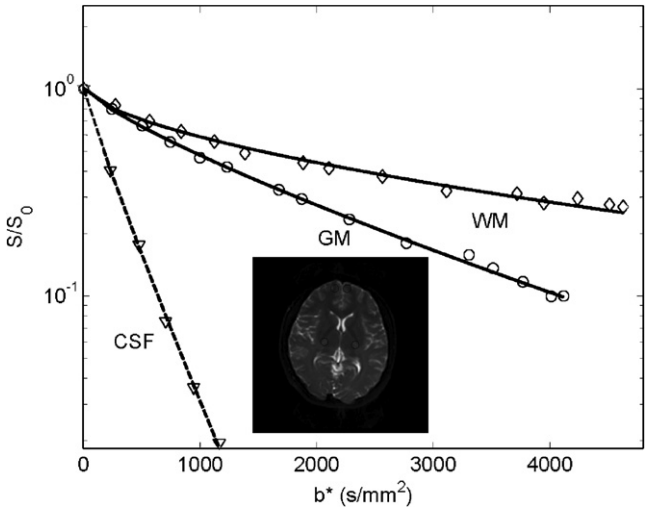

Fig. 7. Normalized signal intensity plotted versus b^*, where $b^* = (\gamma G_z\delta)^2\left(\Delta - \frac{2\beta-1}{2\beta+1}\delta\right)$, for selected ROI in white matter, gray matter and cerebrospinal fluid for a human brain. The experimental data were fit to the fractional order stretched exponential model (Eq. (16c)) to determine D_f, β and μ for $\Delta = 42$ ms and $\delta = 32$ ms. The inset is a DW-EPI T_2-weighted image at 3.0 T, TR/TE = 4000/97 ms, FOV = 22 cm × 22 cm, matrix 128 × 72 (zero padded to 256 × 256 during image reconstruction), in plane resolution = 1.72 mm × 3.05 mm and slice thickness = 4 mm.

5. Discussion

NMR relaxation and diffusion phenomena are often described by functions that exhibit power law behavior in time or frequency (e.g., $\omega^{-\alpha}$, $t^{-\alpha}$, $\exp(-t^{\alpha})$, or in this paper, $E_{\alpha}(-t^{\alpha})$). Such results can be derived from the Bloch equation and the physics of diffusion through a generalization of the underlying phenomena—T_1, T_2 relaxation and anomalous diffusion—using fractal modeling and fractional calculus. One rationale for this approach is the desire to incorporate "memory" or long distance spatial correlations in the spin dynamics of heterogeneous materials. This behavior is naturally expressed in the fundamental representation of spin–spin and spin–lattice interactions, as well as in the apparent diffusion coefficient of water by using fractional order differential operators. For example, in relaxation, fractional order dynamics can arise in the spectral density through the autocorrelation function with a fractal order propagator [16], while in diffusion, the anomalous behavior in the mean squared displacement of water molecules $\langle r^2\rangle \sim t^{\alpha}$, follows from the fractional-order, space-time generalization of the diffusion equation. In this paper we have shown that incorporating fractional order space and time derivatives in the Bloch–Torrey equation gives, for simple cases, results whose functional behavior follows fractional order power laws. The usefulness of this approach is not simply through the introduction of extra "fitting" parameters, but manifests itself in a growing understanding of how fractional order operators encode information about the molecular interactions of spin labeled water that is embedded in the structure of polymers, membranes, and the extracellular matrix of cells and tissues. This interpretation follows from viscoelastic, dielectric and optical measurements that confirm fractional order dynamics at the molecular scale, often with a direct role for fractal order geometric models of the supporting matrix or medium [9,10]. A recent example of the success of this approach is the NMR microscopy of the time-fractional diffusion by Klemm et al. [40] which shows how the fractional order exponents can be obtained from the two-dimensional fractal geometry of the percolation surface clusters.

Over the past few years, a number of reports have suggested that the signal intensity in diffusion-weighted images

of biological tissues does not necessarily follow the well-known mono-exponential decay model, especially at high b-values [41–45]. At least two diffusion "compartments" have been identified with distinctive diffusion coefficients that can differ as much as 9- to 10-fold. The distinctive diffusion compartments have been related to intra- and extra-cellular volume fractions with the assumption that the sub-cellular structures and higher concentration of macromolecules inside the cell can considerably slow down the diffusion process. However, the measured slow diffusion compartment fraction is poorly correlated with known cell volume fraction. To resolve this discrepancy, the effect of the cell membrane on diffusion has been considered, which given a much improved correlation between the diffusion measurements and tissue structures [46–48]. The model based on restricted diffusion at or near the cell membrane, however, brings new issues with respect to the cell membrane's permeability to water molecules. All these diffusion studies suggest the limitations with the existing mono or multi-exponential model, which is derived from the classical Bloch–Torrey equation.

Generalization of the phenomenological Bloch equation began with Bloch [49], who with Wangsness in 1953 [50], sought to modify the underlying assumptions for the Bloch equation (e.g., $\mathbf{B}_0 >> \mathbf{B}_1$, $\Delta B_0 << (1/\gamma T_2)$) to further expand its range of applicability. Reviews of this early work can be found in the book by Abragam [1]. Memory effects were also introduced directly into the Bloch equation by Argyres and Kelley [51], and Robertson [52] who applied the method of Zwanzig [53]—an approach also followed more recently by Glöckle and Nonnenmacher [54] to correlate anomalous relaxation with fractional calculus. Roberston, for example, writes the generalized Bloch equation as

$$\frac{\mathrm{d}\mathbf{M}}{\mathrm{d}t} = \gamma \mathbf{M} \times \mathbf{H}(t) - \int_0^t \mathbf{K}(t,t')[\mathbf{M}(t') - \chi_0 \mathbf{H}(t')]\,\mathrm{d}t', \tag{28}$$

where the kernel $K(t,t')$ is simplified to the time-invariant form $K(t,t') = K(t-t')$ and assumed to fall off slowly as t' recedes from t (fading memory) so that the past as well as present values of $\boldsymbol{M}$ are used to determine $\mathrm{d}\boldsymbol{M}/\mathrm{d}t$. Robertson's results reduce to

$$\frac{\mathrm{d}\mathbf{M}}{\mathrm{d}t} = \gamma \mathbf{M} \times \mathbf{H} + \frac{1}{\tau}[\chi \mathbf{H} - \mathbf{M}] \tag{29}$$

for $K(t-t') = \delta(t-t')/\tau$, where $T_1 = T_2 = \tau$. This modification to the Bloch equation was also derived by Wangsness. Extension of the kernel to the power law form

$$K(t-t') = \frac{(t-t')^{\alpha-1}}{\Gamma(\alpha)\tau^{1+\alpha}}, \quad \text{where } \lim_{\alpha \to 0^+} \frac{(t-t')^{\alpha-1}}{\Gamma(\alpha)\tau^{1+\alpha}} = \frac{\delta(t-t')}{\tau} \tag{30}$$

ensures the expected integral order behavior. This kernel gives the fractional order diff-integral equation

$$\frac{\mathrm{d}\mathbf{M}}{\mathrm{d}t} = \gamma \mathbf{M} \times \mathbf{H}(t) - {}_0D_t^{-\alpha}[\mathbf{M}(t) - \chi \mathbf{H}(t)]. \tag{31}$$

More recently, the focus of NMR studies of anomalous diffusion has concentrated on modeling tissues and porous media. Kimmich [16] and Stapf [17], for example, developed non-Gaussian propagators for the description of pulsed field gradient NMR diffusion studies. In these situations, diffusion appears to be anomalous (e.g., $\langle x^2 \rangle \sim t^\gamma$, $0 < \gamma < 2$) when the molecules are confined to a porous medium and the measuring interval is in what Kimmich calls the "scaling window", $a < \sqrt{\langle x^2 \rangle} < \zeta$ where a is a base dimension of the medium and ζ is the correlation length of the pore space. In particular, Kimmich shows that non-Gaussian propagators in one dimension $P(x,t)$ satisfy a fractional order partial differential equation of the form

$${}_0D_t^{1+k} P(x,t) = D_k \frac{\partial^2}{\partial x^2}[P(x,t)], \tag{32}$$

where ${}_0D_t^{1+k}$ is a fractional derivative of order (k+1) and D_k is the generalized diffusion coefficient (units, $\mathrm{mm}^2/(\mathrm{s})^{1+k}$). This equation can be solved analytically for a source concentrated at the $x = 0$ to give

$$P(x,t) = \frac{1}{\sqrt{4\pi D_k t^k}} H_{1,2}^{2,0}\left[\frac{x^2}{4D_k t^k} \,\middle|\, \begin{matrix} \left(1 - \frac{k}{2}, k\right) \\ (0,1), \left(\frac{1}{2}, 1\right) \end{matrix} \right], \tag{33}$$

where $H_{1,2}^{2,0}$ is a Fox function [16,32]. In the limit $\langle x^2 \rangle >> D_k t^k$ this function converges to a stretched Gaussian, and for $k = 1$ it gives the ordinary one-dimensional result

$$P(x,t) = \frac{1}{\sqrt{4\pi D t}} \exp\left[\frac{-x^2}{4Dt}\right]. \tag{34}$$

Most recently Bennett [7,8] and Özarslan [33] demonstrated the advantages of the stretched exponential model for fitting NMR diffusion data from tissues and multicompartment systems. In one study Bennett [7] found that the stretched exponential function, $S(b) = S_0 \exp(-bD)^\alpha$, provided a better fit for rat cortex diffusion data—using α in the range of 0.77–0.82, and D in the range of 6.8–$8.0 \times 10^{-4}\,\mathrm{mm}^2/\mathrm{s}$—than both single and biexponential models. In a second study Bennett [8] found that for measurements in the human brain the stretched exponential model gave values of α that were relatively insensitive to the orientation of the applied field gradients. The authors suggest that maps of α can be used to assess tissue heterogeneity. In a subsequent study Özarslan [33] and co-workers conducted q-space diffusion experiments on suspensions of human red-blood cell ghosts, normal brain and brain tumor autopsy samples. Their results showed, for example, that water diffusion was anomalous with α values less than 1.0. Özarslan's study connected the observed q-space ($\boldsymbol{q} = (2\pi)^{-1}\gamma\delta\boldsymbol{g}$) data with a fractal space model for diffusion in tissue; a result that provides a simple model for anomalous diffusion in a complex medium. In particular, two parameters: d_w, the random walk dimension, and d_s the spectral dimension, were independently estimated and both were found to vary significantly between normal brain and brain tumor tissue (e.g., for $\alpha = 2/d_\mathrm{w}$, they found for

gray matter, $\alpha = 0.850$; for tumor, $\alpha = 0.916$; and for erythrocyte ghosts, $\alpha = 0.996$). Finally, Özarslan, used fractional order modeling of q-space NMR data to extrapolate the signal attenuation curves as

$$E(q,\Delta) = f_1 e^{-uq^2} + f_2 e^{-(vq^2)^{\alpha}} + f_3(1+wq^2)^{-\eta}, \tag{35}$$

where the first term corresponds to Debye relaxation, the second to a stretched exponential (sometimes described as a Kohlrausch–Williams–Watts function), and the third to a Rigaut-type asymptotic functional expression. This model of $E(q,\Delta)$ was shown for erythrocyte ghosts to provide an excellent description of q-space data spanning five orders of magnitude.

In our study we used fractional calculus to generalize the Bloch–Torrey equation. The results demonstrate that fractional order differential operators in space and time yield solutions similar in form to those developed by Özarslan and others. The specific form of the fractional order solutions for the transverse magnetization depends on the applied gradient pulse waveform. Generalization of the spatial Laplacian gives stretched exponential behavior that is different from the classical and stretched exponential results, and includes in addition to the operational order parameter β, the unit preserving space constant μ (with units, m). The differences between our results and those of others is most clearly seen when the attenuation function is expressed in terms of G_z, δ, β and Δ. A summary is provided in Table 2, assuming that $\Delta >> \delta$. Note, that in each case the units of the apparent diffusion coefficient must be adjusted to maintain D values with the units of mm^2/s. Since restricted diffusion arises in situations where b-values ($b = (\gamma G_z \delta)^2 \Delta$) are no longer independent of the manner in which the individual parameters (G_z, δ, Δ) are changed, it is clear that each equation provides a different way to express such behavior. In addition, it also suggests that the conventionally defined b-value may not be the most suitable parameter to characterize the degree of diffusion weighting. The attenuation curves are all written in Table 2, for comparison, directly in terms of b. In Section 4 we compared the behavior of the fractional order model with the predictions of other models, some of which are interconnected. Note, for example, that when $\mu = \sqrt{D\Delta}$ the fractional order result (Case **I**, $\alpha = 1$, β arbitrary) conforms with the curve assumed by Bennett and co-workers [7,8].

The fractional order results expressed in terms of β, Eq. (16c) were used to fit experimental data collected from Sephadex gel, cartilage and brain. When the experimental curves exhibited evidence of restricted diffusion, the β values of the fits always fell below $\beta = 1$, as expected. Also the μ values all appear to increase as the diffusion attenuation curves depart from the expected straight line of the exponential semi-log plot. The behavior of μ is consistent with the definition: $D_F^{\beta} = D_f(\Delta/\mu^2)^{1-\beta}$, and follows directly from its role as a unit-preserving space constant in the Bloch–Torrey equation. Further study of porous materials is needed to better characterize the relationship between μ and the size and distribution of barriers to diffusion. In the same sense that τ identifies a characteristic time scale for NMR signal attenuation, it is likely that μ can be related to the porosity and tortuosity in a more complete model for fractional order molecular dynamics. Future work will investigate further the sensitivity of the curve fits to the parameters β and μ for different experimental situations. The goal of this study was not to develop a best fit expression for the materials studied, but simply to examine a new class of functions from which a better fit to experimental data may be realized. In the case of a simple pulse gradient spin echo experiment, Fig. 3 for example, the fractional order result for the amplitude of the signal at the echo provides a new expression that is different from both the classical result and the fractal diffusion model developed by Kärger and co-workers [14].

Generalization of the Bloch–Torrey equation using a fractional order time derivative was also developed here for completeness. No data is presented to fit the derived expressions, but for the case of a fixed G_z gradient, the expected signal decay curve conforms to both the classical result and to the result derived in the recent study by Widom and Chen [15] for a fractal model of diffusion. In the case of the fractional order time derivative a new time constant τ was introduced to maintain consistency in the units. The results were obtained only under the condition $(t/\tau) < 1$. This assumption is reasonable if τ is assumed to be on the order of T_1, or for situations with long T_2, but not if $\tau \sim \tau_c$, where τ_c is the correlation time for spin rotation. In the long time limit $(t/\tau) > > 1$ different asymptotic expansions for the Mittag-Leffler functions will have to be investigated. Another area of future study is fractional order relaxation. Here, extension of the correlation function $g_{\omega}(\tau)$ from an exponential to either a power law or a Mittag-Leffler function would generalize the free induction decay signal $G(t)$ and the Hahn echo as described by Callaghan [55]. In a similar manner Bryant and others [56–59] have studied power law behavior of the T_1 relaxivity

Table 2
Comparison of the pulse gradient spin echo diffusion attenuation curves for different models

	Diffusion model (G_z, δ, Δ)	Parameter	Diffusion model (b)	Apparent diffusion coefficient
Stejskal–Tanner	$S = S_0 \exp[-(\gamma\ G_z\delta)^2 \Delta D]$	—	$S = S_0\ \exp[-bD]$	D
Kärger	$S = S_0 \exp[-(\gamma G_z\delta)^2 \Delta^{2H} D^{K\ddot{a}}]$	$0 < H < 1$	$S = S_0 \exp[-bD_{ap}^{K\ddot{a}}]$	$D_{ap}^{K\ddot{a}} = D^{K\ddot{a}}/\Delta^{1-2H}$
Magin	$S = S_0 \exp[-(\gamma G_z\delta)^{2\beta}\ \Delta D_f/\mu^{2(1-\beta)}]$	$1/2 < \beta < 1$	$S = S_0 \exp[-b^{\beta} D_F^{\beta}]$	$D_F^{\beta} = D_f(\mu^2/\Delta)^{1-\beta}$
Bennett	$S = S_0\ \exp[-(\gamma G_z\delta)^{2\alpha}\ \Delta^{\alpha} D^{\alpha}]$	$0 < \alpha < 1$	$S = S_0 \exp[-b^{\alpha} D^{\alpha}]$	D^{α}

In this Table Δ represents the time period between gradient pulses in the short pulse approximation ($\Delta \gg \delta$) and $b = (\gamma G_z \delta)^2 \Delta$. The units of D and D_f are mm^2/s, of $D^{K\ddot{a}}$ are mm^2/(s)^{2H}, of D_F^{β} are (mm)$^{2\beta}$/s$^{\beta}$, and of D^{α} are (mm)$^{2\alpha}$/s$^{\alpha}$.

($1/T_1 = A\omega^{-b}$, where A and b are constants) for proteins and polypeptides.

In addition, there is a literature on the analysis of relaxation times (particularly T_2) obtained by fitting data to a continuous distribution of relaxation times rather than a set of discrete relaxation times that is analogous to the stretched exponential diffusion model analysis [60–65]. This approach points to the need to link the new theoretical concepts and mathematical descriptions of anomalous diffusion [66,67] to known physical parameters. The connection between diffusion restricted by boundaries and unrestricted diffusion through periodic microscopic–mesoscopic gradients was studied long ago by Wayne and Cotts [68]. Indeed, restricted diffusion across semi-permeable membranes is along with cellular heterogeneity a likely source of the complexity modeled using fractional calculus in this paper. The fractional order generalization of the Bloch–Torrey equation will ultimately need to be justified through its ability to describe NMR phenomena; however, we should note the success of fractional order dynamics in describing anomalous diffusion [21] and long range interactions in coupled oscillators [69]. These extensions to a fractional order description of relaxation and experimental analysis of pulsed gradient spin echo models are currently underway as we work to further develop the range of this approach to establish its experimental usefulness.

In summary, the description of NMR relaxation and diffusion processes by non-exponential functions has a long and diverse history. The use of the stretched exponential models for fitting the NMR signal attenuation caused by diffusion is just one example of a variety of functions and functional models currently being employed by NMR and MRI researchers. In the case of diffusion, the connection between the parameter α and the intravoxel heterogeneity can be made through statistical, probabilistic and fractal models of tissue, and is now increasingly recognized. Clinical applications of α-weighted diffusion images have been proposed for assessing stroke, cancer progression, and spinal injury. Our results suggest that the underlying models for anomalous diffusion—and perhaps relaxation—can be established directly from the Bloch equation through the application of the tools of fractional calculus. Using these mathematical tools, we may extend the applications of diffusion imaging beyond simply evaluating the apparent diffusion coefficient and stretched exponential constant α, and eventually reveal new parameters related to tissue microenvironment.

Acknowledgments

The authors wish to thank their colleagues at the Center for Magnetic Resonance Research (CMRR) and the Research Resources Center (RRC) at the University of Illinois at Chicago for their assistance in collecting the data used in this research. In particular we would like to thank Dr. Robert Kleps, Director of the NMR Laboratory of the RRC and Dr. Keith R. Thulborn, Director of the CMRR. We also gratefully acknowledge helpful discussions of this work with Om P. Agrawal, Igor Podlubny, Richard W. Briggs, Barjor Gimi, Girish Srinivasan and Donald E. Woessner, as well as the useful comments provided by the anonymous reviewers.

Appendix

The tools of fractional calculus are as old as calculus itself—the first published results are cited in a letter from Leibniz to L'Hospital in 1695 (see the seminal monograph by Oldham and Spanier [70] for an historical survey). However, only relatively recently has the usefulness of fractional calculus been recognized for solving problems in viscoelasticity, electrochemistry and diffusion [9,10,23]. Unfortunately, most mathematical physics and calculus texts do not describe fractional calculus, and advanced texts on fractional calculus [36] are not written for a beginner. Fortunately, new texts e.g., [21,32,33]—highlighting fractional calculus as a tool for the analysis of complex systems—recent conference proceedings [24–26], and special issues of journals [27–31] are bringing the methods of fractional calculus and its applications to a wider audience.

In the present paper two different formalisms for fractional calculus—one spatial and the other temporal—are used. For both approaches we are able to extend integral and differential operators to non-integer order. One can imagine such a generalization in at least three ways: (i) in terms of the algebraic operators commonly used to solve ordinary differential equations (e.g., D, D^3, $D^5, \ldots \Rightarrow D^{1/2}$, $D^{3/2}, D^{5/2}$); (ii) in terms of the Laplace or Fourier transform representation of differentiation, $sf(s)$ or $(j\omega)f(j\omega)$, extended to $s^\alpha f(s)$ or $(j\omega)^\alpha f(j\omega)$; or (iii) in terms of generalized functions where the fractional order derivative is represented as a convolution in the distributional sense [71], for example in time: ${}_0D_t^\alpha f(t) = k^\alpha(t) * f(t)$; or space: $D_x^\beta g(x) = k^\beta(x) * g(x)$, where $k^\alpha(t)$ and $k^\beta(x)$ are simple power law functions, such as $t^{\alpha-1}/\Gamma(\alpha)$, where $\Gamma(\alpha)$ is the gamma function. Each approach has advantages, but each also has restrictions on its range of applicability due to the need to establish the existence, uniqueness, or convergence of the corresponding function or functional under integration.

Because NMR researchers are familiar with Fourier and Laplace transforms, the fractional calculus operators are defined here in the context of these integral transforms. The validity of all operations, the necessary initial conditions, and the assumed behavior of the involved functions all follow from the usual constraints of linearity, causality, and bounded support for images and physical processes. Below is a brief list of definitions for the fractional order operators used in this paper and of the Mittag-Leffler function—a generalized exponential—which often occurs when solving problems in fractional calculus.

Appendix A. Fractional order operators in space (Riesz fractional derivative)

If we consider a well behaved function $y(x)$ on $(-\infty,\infty)$ then we can define its Fourier transformation $y(\xi_x)$ through the integrals [34]:

$$F\{y(x)\} = \hat{y}(\xi_x) = \int_{-\infty}^{\infty} y(x')\mathrm{e}^{\mathrm{i}\xi_x x'}\,\mathrm{d}x',$$

$$y(x) = F^{-1}\{\hat{y}(\xi_x)\} = \frac{1}{2\pi}\int_{-\infty}^{\infty} \hat{y}(\xi_x)\mathrm{e}^{-\mathrm{i}\xi_x x}\,\mathrm{d}\xi_x.$$

In the Fourier domain for $\beta > 0$, we will define the Fourier transform of the fractional order derivative as

$$F\{D_x^\beta y(x)\} = |\xi_x|^\beta F\{y(x)\}.$$

Hence, we can write the Riesz fractional derivative with respect to space [34] as

$$D_x^\beta[y(x)] = F^{-1}\{|\xi_x|^\beta \hat{y}(\xi_x)\} = F^{-1}\{|\xi_x|^\beta F\{y(x)\}\}.$$

In the case of $y(x) = \mathrm{e}^{\mathrm{i}ax}$ since, $F\{\mathrm{e}^{\mathrm{i}ax}\phi(x)\} = \hat{\phi}(\xi_x + a)$ and $F\{1\} = 2\pi\delta(\xi_x)$ where $\delta(\xi_x)$ is the delta function, we find

$$F(\mathrm{e}^{\mathrm{i}ax}) = |\xi_x|^\beta \delta(\xi_x + a).$$

Using the definition of the inverse Fourier transform and the properties of the delta function, we obtain

$$D_x^\beta(\mathrm{e}^{\mathrm{i}ax}) = F^{-1}\{2\pi|\xi_x|^\beta\delta(\xi_x + a)\} = |a|^\beta \mathrm{e}^{\mathrm{i}ax}.$$

Appendix B. Fractional order operators in time (Caputo fractional derivative)

If we consider a well behaved function $y(t)$ on $[0,\infty)$ then we can define its Laplace transformation through the integrals [34]:

$$L\{y(t)\} = \hat{y}(s) = \int_0^{\infty} y(t')e^{-st'}\,\mathrm{d}t',$$

$$y(t) = L^{-1}\{\hat{y}(s)\} = \frac{1}{2\pi\mathrm{i}}\int_{c-\mathrm{i}\infty}^{c+\mathrm{i}\infty} y(s)e^{st}\,\mathrm{d}s.$$

In the Laplace domain for $(0 < \alpha < 1)$, we will define the Caputo fractional order form of the Riemann–Liouville derivative [35] as

$$L\{{}_0{}^C D_t^\alpha y(t)\} = s^\alpha y(s) - s^{\alpha-1}y(0^+).$$

Hence we can write

$${}_0{}^C D_t^\alpha[y(t)] = L^{-1}\{s^\alpha L\{y(t)\}\} - \frac{y(0^+)t^{-\alpha}}{\Gamma(1-\alpha)},$$

where $\Gamma(1-\alpha) = \int_0^\infty e^{-u}u^{-\alpha}du$ is the Gamma function.

In the time domain for $0 < \alpha < 1$, we have

$${}_0{}^C D_t^\alpha[u(t)] = 0,$$

$${}_0{}^C D_t^\alpha[t^k u(t)] = \frac{\Gamma(k+1)t^{k-\alpha}}{\Gamma[k-\alpha+1]} (\text{for } k > 0),$$

$${}_0{}^C D_t^\alpha[E_\alpha(\lambda t^\alpha)u(t)] = \lambda E_\alpha(\lambda t^\alpha).$$

where $u(t)$ is a unit step function at $t = 0^+$.

Appendix C. Mittag-Leffler functions

The Mittag-Leffler function is a generalization of the exponential function e^t that was introduced by the Swedish mathematician G.M. Mittag-Leffler in 1903–1904. The basic properties of the function are given in the monograph by Carpinteri and Mainardi [24] and the books by Podlubny [35], Kilbas et al. [34] and Samko et al. [36]. In this paper three forms of the Mittag-Leffler function are used. Each is defined below in terms of a power series representation involving the Gamma function, defined by the integral

$$\Gamma(z) = \int_0^\infty e^{-u}u^{z-1}\,\mathrm{d}u.$$

(1) Single-parameter Mittag-Leffler

$$E_\alpha(t) = \sum_{k=0}^{\infty}\frac{t^k}{\Gamma(\alpha k+1)} \qquad (\alpha, \text{real} > 0),$$

$$E_1(t) = e^t, \quad \text{since } \Gamma(k+1) = k!;$$

$$E_2(t) = \cosh\sqrt{t}; \quad E_2(-t) = \cos\sqrt{t}.$$

(2) Two-parameter Mittag-Leffler

$$E_{\alpha,\beta}(t) = \sum_{k=0}^{\infty}\frac{t^k}{\Gamma(\alpha k+\beta)} \quad (\alpha, \text{real} > 0; \beta, \text{real} > 0),$$

$$E_{1,2}(t) = \frac{e^t - 1}{t}; \quad E_{2,2}(t) = \frac{\sinh\sqrt{t}}{\sqrt{t}}; \quad E_{2,1}(t) = \cosh\sqrt{t}.$$

.

(3) Generalized two-parameter Mittag-Leffler

$$E^\rho_{\alpha,\beta}(t) = \sum_{k=0}^{\infty}\frac{(\rho)_k t^k}{\Gamma(\alpha k+\beta)k!}, \quad \text{where}$$

$$(\rho)_k = \frac{\Gamma(\rho+k)}{\Gamma(\rho)} \quad (\rho, \text{real} > 0),$$

$$E^1_{\alpha,\beta}(t) = E^{(t)}_{\alpha,\beta};$$

$$\left(\frac{\mathrm{d}}{\mathrm{d}t}\right)^n [E_{\alpha,\beta}(t)] = n!E^{n+1}_{\alpha,\beta+\alpha n}(t) \quad \text{for } n = 1,2,3,\ldots$$

$$E^\rho_{1,\beta}(t) = \frac{1}{\Gamma(\beta)}\,{}_1F_1(\rho,\beta,t).$$

where ${}_1F_1(\rho,\beta,t)$ is the Kummer confluent hypergeometric function.

A useful property of the Mittag-Leffler function is its behavior under the Laplace transformation. The following expressions are valid for real $s > |\lambda|^{1/\alpha}$:

$$L\{E_\alpha(-\lambda t^\alpha)\} = \frac{s^{\alpha-1}}{s^\alpha+\lambda};$$

$$L\{t^{\alpha-1}E_{\alpha,\alpha}(-\lambda t^\alpha)\} = \frac{1}{s^\alpha+\lambda};$$

$$L\{t^{\beta-1}E_{\alpha,\beta}(-\lambda t^\alpha)\} = \frac{s^{\alpha-\beta}}{s^\alpha+\lambda}; \; L\{t^{\beta-1}E^\rho_{\alpha,\beta}(-\lambda t^\alpha)\} = \frac{s^{\alpha\rho-\beta}}{(s^\alpha+\lambda)^\rho}.$$

Appendix D. Leibniz rule for fractional derivatives

The nth derivative of the product $\phi(t)f(t)$ is given by the Leibniz rule

$$\frac{\mathrm{d}^n}{\mathrm{d}t^n}[\phi(t)f(t)] = \sum_{k=0}^{n} \binom{n}{k} \phi^{(k)}(t) f^{(n-k)}(t),$$

$$\text{where } \binom{n}{k} = \frac{n!}{k!(n-k)!}.$$

Thus,

$$\frac{\mathrm{d}^3}{\mathrm{d}t^3}[\phi(t)f(t)] = \binom{3}{0}\phi^{(0)}(t)f^{(3)}(t) + \binom{3}{1}\phi^{(1)}(t)f^{(2)}(t) + \binom{3}{2}\phi^{(2)}(t)f^{(1)}(t) + \binom{3}{3}\phi^{(3)}(t)f^{(0)}(t),$$

$$\frac{\mathrm{d}^3}{\mathrm{d}t^3}[\phi(t)f(t)] = \phi(t)\frac{\mathrm{d}f^3(t)}{\mathrm{d}t^3} + 3\frac{\mathrm{d}\phi(t)}{\mathrm{d}t}\frac{\mathrm{d}^2 f(t)}{\mathrm{d}t} + 3\frac{\mathrm{d}^2\phi(t)}{\mathrm{d}t^2}\frac{\mathrm{d}f(t)}{\mathrm{d}t} + \frac{\mathrm{d}^3\phi(t)f(t)}{\mathrm{d}t^3}.$$

In fractional calculus the Leibniz rule for the αth order derivative can be written as

$${}_0D_t^{\alpha}[\phi(t)f(t)] = \sum_{k=0}^{\infty} \binom{\alpha}{k} \phi^{(k)}(t)\,{}_0D_t^{\alpha-k} f(t),$$

where $\binom{\alpha}{k} = \frac{\Gamma(\alpha+1)}{k!\Gamma(\alpha-k+1)}$. Such a series representation is only an approximation. When this approach is used, one should estimate the error of the approximation. In this case [33], if both $\phi(t)$ and $f(t)$ and all their derivatives are continuous on the interval $[0, t]$, and since we know that ${}_0{}^{C}D_t^{\alpha} f(t) = {}_0D_t^{\alpha}[f(t) - f(0^+)]$ for $0 < \alpha < 1$, [34] we can apply the Leibniz rule to the Caputo fractional order derivative since, if $f(t)$ and its derivatives are continuous on $[0, t]$ then $f(t) - f(0^+)$ will also satisfy these conditions. Note that when $\alpha < 0$, the series terms involve the usual Riemann–Liouville fractional integral. Thus, in place of the finite series of terms that occurs in integer order calculus, in fractional calculus an infinite series of terms arises. Writing out the first few terms of this expansion gives

$${}_0{}^{C}D_t^{\alpha}[\phi(t)f(t)] = \binom{\alpha}{0}\phi(t)\,{}_0{}^{C}D_t^{\alpha} f(t) + \binom{\alpha}{1}\phi^{(1)}(t)\,{}_0{}^{C}D_t^{\alpha-1} f(t) + \binom{\alpha}{2}\phi^{(2)}(t)\,{}_0{}^{C}D_t^{\alpha-2} f(t) + \binom{\alpha}{3}\phi^{(3)}(t)\,{}_0{}^{C}D_t^{\alpha-3} f(t) + \cdots$$

where

$$\binom{\alpha}{0} = 1, \binom{\alpha}{1} = \alpha, \binom{\alpha}{2} = \frac{\alpha(\alpha-1)}{2\cdot 1}, \binom{\alpha}{3} = \frac{\alpha(\alpha-1)(\alpha-2)}{3\cdot 2\cdot 1}, \cdots$$

In Eq. (22) in the text we truncated this series after the first two terms.

In general this series takes the form

$${}_0{}^{C}D_t^{\alpha}[\phi(t)f(t)] = \phi(t)\,{}_0{}^{C}D_t^{\alpha} f(t) + \frac{\alpha \mathrm{d}\phi(t)}{\mathrm{d}t}\,{}_0D_t^{\alpha-1} f(t) \left[1 + \frac{\frac{\alpha(\alpha-1)}{2}\frac{\mathrm{d}^2\phi(t)}{\mathrm{d}t^3}\,{}_0D_t^{\alpha-2} f(t)}{\alpha\frac{\mathrm{d}\phi(t)}{\mathrm{d}t}\,{}_0D_t^{\alpha-1} f(t)} + \frac{\frac{\alpha(\alpha-1)(\alpha-2)}{6}\frac{\mathrm{d}^3\phi(t)}{\mathrm{d}t^3}\,{}_0D_t^{\alpha-3} f(t)}{\alpha\frac{\mathrm{d}\phi(t)}{\mathrm{d}t}\,{}_0D_t^{\alpha-1} f(t)} + \cdots\right].$$

which can be written as

$${}_0{}^{C}D_t^{\alpha}[\phi(t)f(t)] = \phi(t)\,{}_0{}^{C}D_t^{\alpha} f(t) + \frac{\alpha \mathrm{d}\phi(t)}{\mathrm{d}t}\,{}_0{}^{C}D_t^{\alpha-1} f(t)[1 + M + N + \cdots],$$

where the terms M and N represent the indicated fractions. Neglecting M, N and the higher order terms gives the solution $\phi(t) = A(t) = \exp[-B(t/\tau)^{3\alpha}]$ and $f(t) = E_{\alpha}[-\mathrm{i}\gamma z G_z \tau(t/\tau)^{\alpha}]$. Using these results, substitution of the stretched exponential and the single parameter Mittag-Leffler function into the series terms M and N, it can be shown that for $1/3 < \alpha < 1$, both M and N approach zero in the limit when $t << \tau$. The lower boundary on α is required to satisfy the necessary condition that $\phi(t)$ be continuous on $[0, t]$.

References

[1] A. Abragam, Principles of Nuclear Magnetism, Oxford University Press, New York, 2002.

[2] E.M. Haacke, R.W. Brown, M.R. Thompson, R. Venkatesan, Magnetic Resonance Imaging: Physical Principles and Sequence Design, Wiley, New York, 1999.

[3] D. Le Bihan, Diffusion and Perfusion Magnetic Resonance Imaging: Applications to Functional MRI, Raven Press, New York, 1995.

[4] M.A. Bernstein, K.F. King, X.J. Zhou, Handbook of MRI Pulse Sequences, Elsevier Academic Press, Burlington, MA, 2004.

[5] T. Vaughan, L. DelaBarre, C. Snyder, J. Tian, C. Akgun, D. Shrivastava, W. Liu, C. Olson, G. Adriany, J. Strupp, P. Andersen, A. Gopinath, P.F. van de Moortele, M. Garwood, K. Ugurbil, 9.4 T human MRI: preliminary results, Magn. Reson. Med. 56 (2006) 1274–1282.

[6] M.P. McDougall, S.M. Wright, 64-channel array coil for single echo acquisition magnetic resonance imaging, Magn. Reson. Med. 54 (2005) 386–392.

[7] K.M. Bennett, K.M. Schmainda, R.T. Bennett, D.B. Rowe, H. Lu, J.S. Hyde, Characterization of continuously distributed cortical water diffusion rates with a stretched-exponential model, Magn. Reson. Med. 50 (2003) 727–734.

[8] K.M. Bennett, J.S. Hyde, K.M. Schmainda, Water diffusion heterogeneity index in the human brain is insensitive to the orientation of applied magnetic field gradients, Magn. Reson. Med. 56 (2006) 235–239.

[9] R. Hilfer, Applications of Fractional Calculus in Physics, World Scientific, Singapore, River Edge, NJ, 2000.

[10] B.J. West, M. Bologna, P. Grigolini, Physics of Fractal Operators, Springer, New York, 2003.

[11] J.R. Banavar, M. Lipsicas, J.F. Willemsen, Determination of the random-walk dimension of fractals by means of NMR, Phys. Rev. B. Condens. Matter 32 (1985) 6066.

[12] G. Jug, Theory of NMR field-gradient spectroscopy for anomalous diffusion in fractal networks, Chem. Phys. Lett. 131 (1986) 94–97.

[13] J. Kärger, G. Vojta, On the use of NMR pulsed field-gradient spectroscopy for the study of anomalous diffusion in fractal networks, Chem. Phys. Lett. 141 (1987) 411–413.

[14] J. Kärger, H. Pfeifer, G. Vojta, Time correlation during anomalous diffusion in fractal systems and signal attenuation in NMR field-gradient spectroscopy, Phys. Rev. A 37 (1988) 4514–4517.
[15] A. Widom, H.J. Chen, Fractal Brownian motion and nuclear spin echoes, J. Phys. A 28 (1998) 1243–1247.
[16] R. Kimmich, Strange kinetics, porous media, and NMR, Chem. Phys. 284 (2002) 253–285.
[17] S. Stapf, NMR investigations of correlations between longitudinal and transverse displacements in flow through random structured media, Chem. Phys. 284 (2002) 369–388.
[18] R. Metzler, T.F. Nonnenmacher, Space- and time-fractional diffusion and wave equations, fractional Fokker–Planck equations, and physical motivation, Chem. Phys. 284 (2002) 67–90.
[19] R. Gorenflo, F. Mainardi, D. Moretti, G. Pagnini, P. Paradisi, Discrete random walk models for space-time fractional diffusion, Chem. Phys. 284 (2002) 521–541.
[20] B.J. West, T.F. Nonnenmacher, An ant in a gurge, Phys. Lett. A 278 (2001) 255–259.
[21] R. Metzler, J. Klafter, The random walk's guide to anomalous diffusion: a fractional dynamics approach, Phys. Rep. 339 (2000) 1–77.
[22] R. Metzler, J. Klafter, The restaurant at the end of the random walk: recent developments in the description of anomalous transport by fractional dynamics, J. Phys. A: Math. Gen. 37 (2004) R161–R208.
[23] R.L. Magin, Fractional Calculus in Bioengineering, Begell House, CT, 2006.
[24] A. Carpinteri, F. Mainardi, Fractals and Fractional Calculus in Continuum Mechanics, Springer, Wien, New York, 1997.
[25] A. Le Mehaute, J.A.T. Machado, J.C. Trigeassou, J. Sabatier, Fractional Differentiation and its Applications, Ubooks Verlag, Diedorf, 2005.
[26] J.A.T. Machado (Ed.), Fractional differentiation and its applications, in: Proceedings of the International Federation of Automatic Control 2nd IFAC Workshop, Porto, Portugal, 2006.
[27] R. Hilfer, R. Metzler, A. Blumen, J. Klafter, Special issue on strange kinetics, Chem. Phys. 284 (2002) 1–541.
[28] J.A.T. Machado, Special issue on fractional order calculus and its applications, Nonlinear Dynamics 29 (2002) 1–385.
[29] M.D. Ortigueira, J.A.T. Machado, Special issue on fractional signal processing and applications, Signal Proc. 83 (2003) 2285–2480.
[30] O.P. Agrawal, Symposium on fractional derivatives and applications in engineering and sciences, in: ASME International Design Engineering Technical Conference, Chicago, IL, 2003.
[31] M.D. Ortigueira, J.A.T. Machado, Special section: Fractional calculus applications in signals and systems, Signal Proc. 86 (2006) 2503–3094.
[32] M. Kopf, R. Metzler, O. Haferkamp, T.F. Nonnenmacher, NMR studies of anomalous diffusion in biological tissues: experimental observation of Levy stable processes, in: G.A. Losa, D. Merlini, T.F. Nonnenmacher, E.R. Weibel (Eds.), Fractals in Biology and Medicine, vol. II, Birkhauser, Basel, 1998, pp. 345–364.
[33] E. Ozarslan, P.J. Basser, T.M. Shepherd, P.E. Thelwall, B.C. Vemuri, S.J. Blackband, Observation of anomalous diffusion in excised tissue by characterizing the diffusion-time dependence of the MR signal, J. Magn. Reson. 183 (2006) 315–323.
[34] A.A. Kilbas, H.M. Srivastava, J.J. Trujillo, Theory and Applications of Fractional Differential Equations, Elsevier, Amsterdam, 2006.
[35] I. Podlubny, Fractional Differential Equations: An Introduction to Fractional Derivatives, Fractional Differential Equations, to Methods of their Solution and some of their Applications, Academic Press, San Diego, 1999.
[36] S.G. Samko, A.A. Kilbas, O.I. Marichev, Fractional Integrals and Derivatives: Theory and Applications, Gordon and Breach, Switzerland, 1993.
[37] X. Zhou, J.K. Maier, S.J. Huff, H.G. Reynolds, Method and apparatus for producing diffusion-weighted MR images, US Patent 6, 323, 646, November 27, 2001.
[38] J.J. More, The Levenberg–Marquardt algorithm: Implementation and Theory, in: G.A. Watson (Ed.), Numerical Analysis, Lecture Notes in Mathematics, vol. 630, Springer, Heidelberg, 1977, pp. 105–116.
[39] J. Buckwalter, T. Einhorn, S. Simon, Orthopedic Basic Science, Biology and Biomechanics of the Musculoskeletal System, American Academy of Orthopedic Surgeons, Rosemont, IL, 2000.
[40] A. Klemm, R. Metzlerand, R. Kimmich, Diffusion on random-site percolation clusters: theory and NMR microscopy experiments with model objects, Phys. Rev. E 65 (2002) 021112-1–021112-4.
[41] C.A. Clark, D. Le Bihan, Water diffusion compartmentation and anisotropy at high b values in the human brain, Magn. Reson. Med. 44 (2000) 852–859.
[42] R.V. Mulkern, H. Gudbjartsson, C. Westin, H.P. Zengingonul, W. Gartner, C.R.G. Guttmann, R.L. Robertson, W. Kyriakos, R. Schwartz, D. Holtzman, F.A. Jolesz, S.E. Maier, Multi-component apparent diffusion coefficients in human brain, NMR in Biomed. 12 (1999) 51–62.
[43] S.C. Grant, D.L. Buckley, S. Gibbs, A.G. Webb, S.J. Blackband, MR microscopy of multicomponent diffusion in single neurons, Magn. Reson. Med. 46 (2001) 1107–1112.
[44] B.A. Inglis, E.L. Bossart, D.L. Buckley, E.D. Wirth III, T.H. Mareci, Visualization of neural tissue water compartments using biexponential diffusion tensor MRI, Magn. Reson. Med. 45 (2001) 580–587.
[45] R.J. Milman, X.J. Zhou, Improved correlation between diffusion parameters and cell volume fraction in high-resolution diffusion-weighted images, in: Proc. Int'l. Soc. Magn. Reson. Med. 11th Meeting, Toronto, Canada, 2003, p. 2265.
[46] J.V. Sehy, L. Zhao, J.Q. Xu, H.J. Rayala, J.J. H Ackerman, J.J. Neil, Effects of physiologic challenge on the ADC of intracellular water in the Xenopus oocyte, Magn. Reson. Med. 52 (2004) 239–247.
[47] J.D. Quirk, G.L. Bretthorst, T.Q. Duong, A.Z. Snyder, C.S. Springer, J.J. H Ackerman, J.J. Neil, Equilibrium water exchange between the intra- and extracellular spaces of mammalian brain, Magn. Reson. Med. 50 (2003) 493–499.
[48] Z. Ababneh, H. Beloeil, C.B. Berde, G. Gambarota, S.E. Maier, R.V. Mulkern, Biexponential parameterization of diffusion and T_2 relaxation decay curves in a rat muscle edema model: decay curve components and water compartments, Magn. Reson. Med. 54 (2005) 524–531.
[49] F. Bloch, Nuclear induction, Phys. Rev. (1946) 460–474.
[50] R.K. Wangsness, F. Bloch, The dynamical theory of nuclear induction, Phys. Rev. (1953) 728–739.
[51] P.N. Argyres, P.L. Kelley, Theory of spin resonance and relaxation, Phys. Rev. 134 (1964) A98–A111.
[52] B. Robertson, Equations of motion of nuclear magnetism, Phys. Rev. 153 (1967) 391–403.
[53] R. Zwanzig, Ensemble method in the theory of irreversibility, J. Chem. Phys. 33 (1960) 1338–1341.
[54] W.G. Glöckle, T.F. Nonnenmacher, Fractional relaxation and the time–temperature superposition principle, Rheol. Acta 33 (1994) 337–343.
[55] P.T. Callaghan, Principles of Nuclear Magnetic Resonance Microscopy, Oxford Press, UK, 2004.
[56] J.P. Korb, R.G. Bryant, The physical basis for the magnetic field dependence of proton spin–lattice relaxation rates in proteins, J. Chem. Phys. 115 (2001) 10964–10974.
[57] J.P. Korb, R.G. Bryant, The magnetic field dependence of T1, Magn. Reson. 48 (2002) 21–26.
[58] J.P. Korb, R.G. Bryant, Noise and functional protein dynamics, Biophys. J. 89 (2005) 2685–2692.
[59] J.P. Korb, G. Diakova, R.G. Bryant, Paramagnetic relaxation of protons in rotationally immobilized proteins, J. Chem. Phys. 124 (2006) 134910.
[60] M.T. Bronskill, G.E. Santyr, B. Walters, R.M. Henkelman, Analysis of discrete T-2 components of NMR relaxation for aqueous-solutions in hollow-fiber capillaries, Magn. Reson. Med. 31 (1994) 611–618.

[61] R. Harrison, M.J. Bronskill, R.M. Henkelman, Magnetization-transfer and T-2 relaxation components in tissue, Mag. Reson. Med. 33 (1995) 490–496.
[62] M.F. Ochs, R.S. Stoyanova, T.R. Brown, W.D. Rooney, C.S. Springer, Differences in T1 distributions between normal volunteers and MS patients identified by Bayesian decomposition relaxographic imaging, Radiology 217 (354) (2000) 183.
[63] J.-H. Lee, C. Labadie, C.S. Springer, G.S. Harbison, Two-dimensional inverse Laplace transform NMR: Altered relaxation times allow detection of exchange correlation, J. Am. Chem. Soc. 115 (1993) 7761–7764.
[64] K.P. Whittall, A.L. MacKay, Quantitative interpretation of NMR relaxation data, J. Magn. Reson. 84 (1989) 134–152.
[65] A.E. English, K.P. Whittall, M.L. Joy, R.M. Henkelman, Quantitative two-dimensional time correlation relaxometry, Magn. Reson. Med. 22 (1991) 425–434.
[66] A.E. Sitnitsky, G.G. Pimenov, A.V. Anisimov, Spin–lattice NMR relaxation by anomalous translational diffusion, J. Magn. Reson. 172 (2005) 48–55.
[67] W. Chen, Time–space fabric underlying anomalous diffusion, Chaos Solit. Fract. 28 (2006) 923–929.
[68] R.C. Wayne, R.M. Cotts, Nuclear-magnetic-resonance study of self-diffusion in a bounded medium, Phys. Rev. 151 (1966) 264–272.
[69] V.E. Tarasov, G.M. Zaslavsky, Fractional dynamics of coupled oscillators with long-range interaction, Chaos 16 (2006) 023110-1–023110-12.
[70] K.B. Oldham, J. Spanier, The Fractional Calculus; Theory and Applications of Differentiation and Integration to Arbitrary Order, Academic Press, New York, 1974.
[71] A.I. Saichev, W.A. Woyczynski, Distributional and Fractal Calculus, Integral Transforms and WaveletsDistributions in the Physical and Engineering Sciences, vol. I, Birkhäuser, Boston, 1997.